Dalton Transactions

ROYAL SOCIETY OF CHEMISTRY

PAPER

View Article Online
View Journal | View Issue

Cite this: *Dalton Trans.*, 2026, **55**, 4977

Amidines: a deeper look at the archetypal pro-ligand

Matthew de Vere-Tucker, Imogen Squire, Michelangelo Tritto, Rohil Anandkar, Tayyibah Syeda, Divia Uthayan, Gabrielle Aguila, Lygia Silva de Moraes and Clare Bakewell *

Amidinates ($[R_1NC(R_2)NR_3]^-$) are versatile and ubiquitous ligands in inorganic and main group chemistry, due to their anionic, bidentate nature and easy tunability. Herein we present the synthesis of 23 bulky *N*-aryl substituted aminidinate ligands *via* three different synthetic routes: 1. condensation reaction in the presence of PPSE (polyphosphric acid trimethylsilylester); 2. the treatment of a carbodiimide with a lithium salt, and 3. the sequential addition of anilines to an acyl chloride and then to the resultant imidoyl chloride. These synthetic routes have been compared and critically analysed. The stabilising properties of the ligands were next probed through complexation with aluminium ($AlH_3{\cdot}NMe_3$), where it was found that the bulkier ligands afford aluminium dihydride complexes, whereas the less bulky ligands instead afford bis-ligated aluminium monohydride complexes. Finally, we utilised computational methods to further explore the steric and electronic properties of these ligands, highlighting the differing effects of different substitution patterns.

Received 2nd February 2026,
Accepted 2nd March 2026

DOI: 10.1039/d6dt00276e

rsc.li/dalton

Introduction

Amidinates are one of the most ubiquitous ligand types in molecular inorganic chemistry: monoanionic supporting ligands which usually form bidentate chelates with transition metal, f-block or main group centres, leading to 4-memembered ring systems (Fig. 1a).[1–5] Despite being prevalent in the chemical literature for decades the structural motif remains a familiar sight, where, amongst other applications, they have found great utility in the stabilisation of low valent metal centres such as Si^{II}, Ge^{II} and dihydrodialanes.[6–11] Recently, amidinate ligands have enabled isolation of an aromatic tetrasilacyclobutadiene dication and a lutetium dinitrogen complex, from which N_2 can be further functionalised (Fig. 1b).[12,13]

Amidines (the amidinate pro-ligand, $R_1NC(R_2)N(H)R_3$) are highly modular, with a wide range of substitutions possible at both the nitrogen (*N*-) atoms (R_1 and R_3 substitution) and the bridge head carbon (*C*-) atom (R_2 substitution, Fig. 1a). These substituents can be aromatic, aliphatic or a combination of the two, leading to a host of accessible symmetric and asymmetric ligand motifs. Upon coordination, this allows the sterics, and to some extent the electronics, of the element centre to which the amidine pro-ligand is bound to be tuned to suit a particular purpose, an attractive proposition for the molecular inorganic chemist. This ready, and remarkably easy, tunability makes amidines relatively unique, certainly amongst related monoanionic bidentate ligand systems often utilised in main group chemistry.

The scope of this tunability is also notable; multidentate ligands with one or more anionic binding sites and pro-ligands with pendant arms, which can provide additional donor groups, are accessible from the basic ligand scaffold.[14,15] In addition, amidinates exhibit a range of binding modes,[2] with this flexibility implicated in the stabilisation of species in a range of oxidation states.[16]

Over the last five years our research group has been combining amidine pro-ligands with main group elements, using

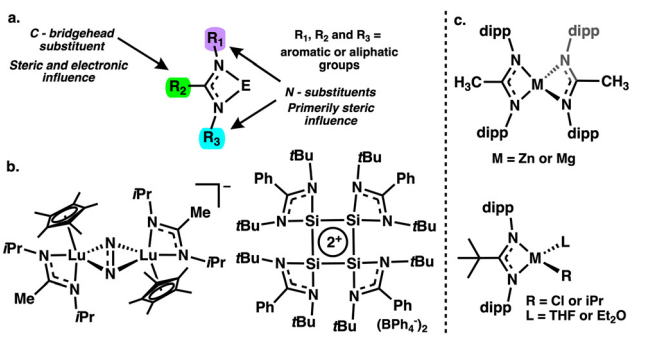

Fig. 1 a. Amidinate ligand substituents b. Recent examples of unique amidinate stabilised species c. The effects substitution at the *C*-bridgehead position on coordination to magnesium and zinc centres.

Department of Chemistry, King's College London, 7 Trinity Street, London, SE1 1DB, UK. E-mail: clare.bakewell@kcl.ac.uk

them to kinetically stabilise reactive metal centres. This has included the isolation of magnesium and aluminium hydrides, for which we have probed the effects of the ligand on both solution structure and catalysis.[17,18] More recently, we have been investigating amidinate-stabilised low-valent aluminium compounds, isolating Al^{I} species with unique trimeric[19] and masked Al^{I} structures, the latter of which forms *via* a redox equilibrium network.[20,21] In both cases, Al^{III} hydrides and iodides are key precursors to the final low oxidation states species.

The utility we have found in this rather simple ligand system has led us to explore a wide range of structural modifications, which suit our synthetic needs. In this pursuit, we have noted two significant shortfalls in the chemical literature.

Firstly, there are three main synthetic routes used to access amidines (*vide infra*); some are more synthetically useful than others and the choice of method can depend on the desired R-groups. Whilst widely reported, we have found reliable amidine syntheses to be scattered amongst the literature and a significant resource that collates and evaluates contrasting synthetic methods is lacking.

Secondly, it is well documented that the effects of substitution at *N*-(R_1 and R_3) and *C*-(R_2) can be significant, sometimes leading to dramatically different products. For example, smaller ligands often led to homoleptic species whereas more sterically demanding ligands can allow for kinetic stabilisation of heteroleptic species. This was observed in a series of zinc and magnesium compounds reported by Gibson and co-workers, where when R_2 = Me bis-ligated homoleptic complexes were formed, but when R_2 = *t*Bu heteroleptic species were isolated (R_1 = R_3 = dipp) (Fig. 1c).[22] Another example from Boeré and co-workers, which also investigated substitution at R_2 (CF_3-, 4-$CH_3(C_6H_4)$- and 4-$OCH_3(C_6H_4)$), noted the pro-ligands had significantly different solution and solid-state structures.[23] There are also studies which draw comparisons between substituent effects and catalytic reactivity. For example, Ma and co-workers have investigated a series of mono-ligated aluminium compounds for the ring-opening polymerisation of lactide, varying R_1. Here, electron withdrawing substituents led to the most efficient catalysts.[24] These studies, however, nearly always focus on a small number of examples, and we have found systematic studies that address substituent effects on coordination across a significant number of compounds absent from the literature. This is particularly true for more subtle structural changes, often at R_2, which *can* have profound effects on the structure and reactivity of resultant compounds.

As such, we embarked on creating a resource that collates the syntheses of amidine pro-ligands and evaluates different synthetic routes under a standard set of experimental conditions. Furthermore, we seek to use these compounds to probe the effects of ligand substitution on coordination in a systematic and informative way. Ultimately, we aim to create a reference for chemists wishing to utilise, replicate or adapt amidine syntheses in their research. As aluminium (Al) complexes have been used previously to "benchmark" amidine ligands,[25,26] and given our own research interests in this area, we opted to evaluate the coordination chemistry of the amidine pro-ligands *via* coordination with an Al precursor.

Results and discussion

Ligand synthesis

It should be noted that the pro-ligands and associated coordination complexes presented herein have been chosen to advance our own research endeavours. Therefore, the adaptations discussed will focus on the nuance of substituent effects within a sterically demanding ligand framework. The modifications targeted can be split into two classes. The first includes variation of *N*-aryl groups (R_1 and R_3, Fig. 1a), with the aim of quantifying the effects of moderate steric changes in these flanking substituents, as well as asymmetry, on the coordination sphere. The second class of modification focusses on varying substitution at the *C*-bridgehead position (R_2, Fig. 1a). A variety of substituted aryl groups and sterically demanding aliphatic substituents will serve to highlight the importance of this apical position.

To achieve the desired range of compounds three different synthetic routes have been utilised (Scheme 1); depending on the substitution arrangement in the resultant pro-ligand, one or more of these routes may be applicable. Pro-ligands **1–23** are shown in Fig. 2.

The first route sees the treatment of 2.1 equivalents of the aniline with 1 equivalent of the chosen carboxylic acid. The reaction is conducted neat, in freshly prepared polyphosphoric acid siloxyester (PPSE) at 170 °C overnight and is followed by an aqueous basic workup (Scheme 1, route 1).[27–31]

Route 2 involves reaction of a slight excess of an aryl or alkyl lithium (1.1 equivalents) with 1 equivalent of a carbodiimide in diethyl ether at 0 °C. After overnight stirring the lithium salt of the ligand can be isolated, or the reaction can be quenched with water to afford the pro-ligand (Scheme 1, route 2).[32]

The third and final route (route 3) follows a stepwise synthesis; initial treatment an appropriate aroyl or acetyl chloride with 1 equivalent of aniline leads to the formation of a second-

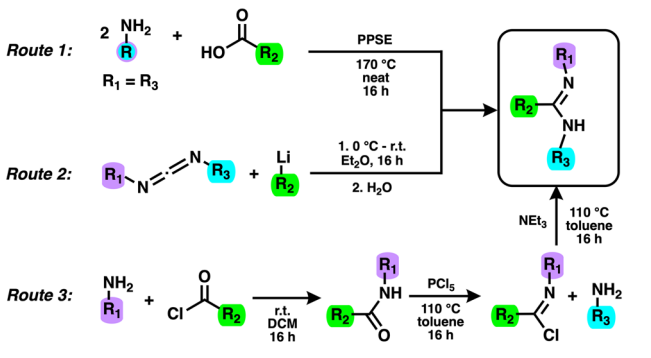

Scheme 1 Three different synthetic routes to the formation of amidine pro-ligands.

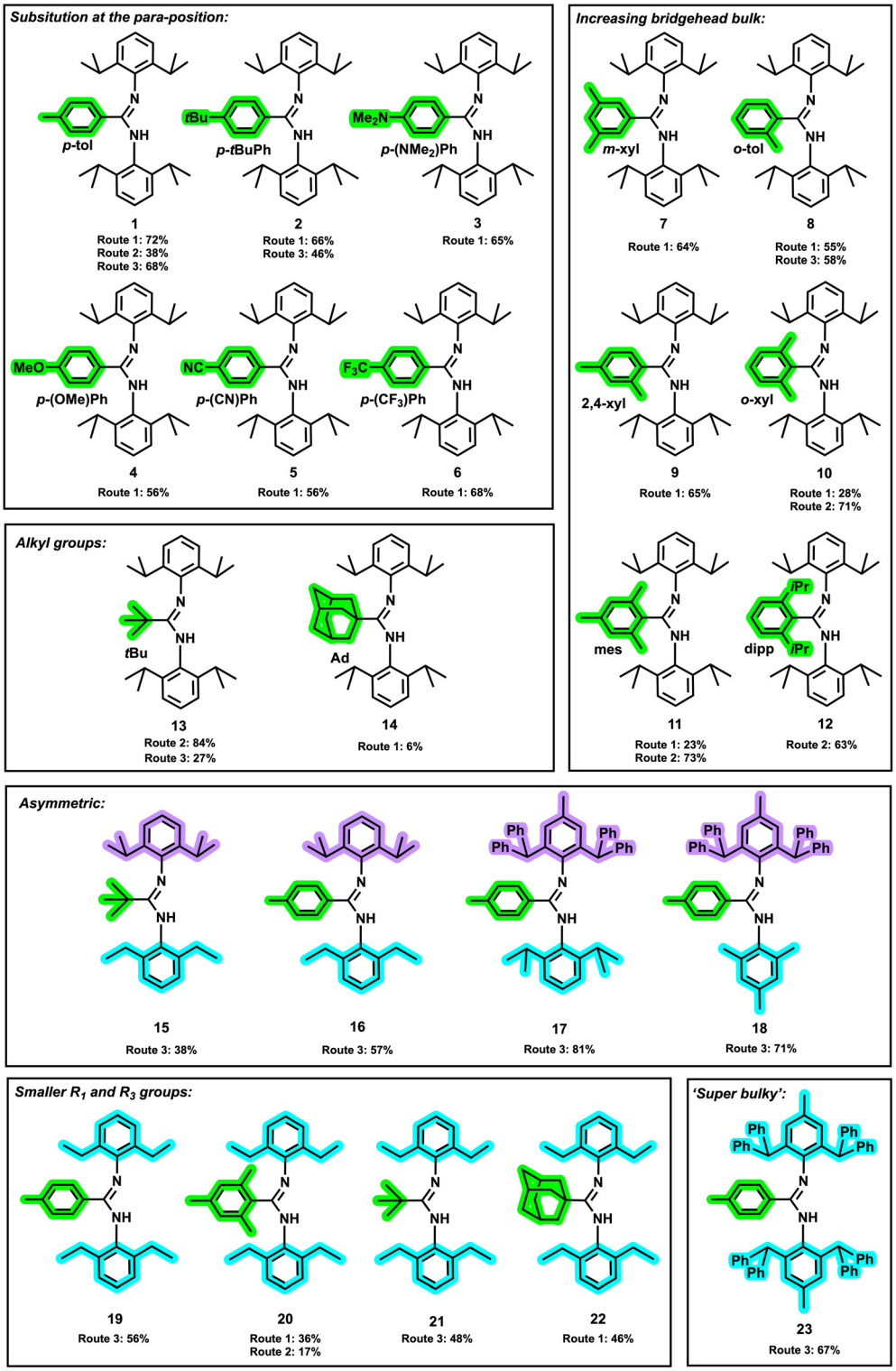

Fig. 2 Amidine ligands and the routes by which they have been isolated. *Note*: route 3 overall yield reported over 2-synthetic steps.

ary amide intermediate. Subsequent chlorination with phosphorous pentachloride (PCl_5) leads to *in situ* formation of the imidoyl chloride, which is reacted directly with a second equivalent of aniline in the presence of triethyl amine, leading to the pro-ligand after neutralisation during work-up (Scheme 1, route 3).[23]

The three respective routes offer competing benefits and disadvantages; we will discuss these respective pathways in the

context of our own research. Some pro-ligand syntheses have been previously reported, by our group or others, and have been included here for completeness. However, all results reported herein are based on data from our own experiments, under standardised synthetic conditions. The pro-ligands **1–23** were prepared using one or more routes (Fig. 2).‡

The principal benefit to route 1 is the one-pot and one-step synthesis; this has been previously discussed by Kays and co-workers.[31] The requirement for high temperatures and neat acidic condition are offset by the good yields afforded by the synthesis. When the *N*-substituents ($R_1 = R_3$) are either diethylphenyl or diisopropylphenyl groups, yields are consistently around 60–70% for a wide range of aromatic *C*-substituents (R_2) [**1–9** and **19**].[31] However, in our hands the yields afforded by this route significantly decrease when the *C*-substituent becomes more sterically hindered. Specifically, aromatic substituents with double *ortho*-substitution [**10–11** and **20**] saw the yield drop to 25–35%. Despite efforts to change reaction conditions, unreacted starting materials or benzamide (mono-addition product) were observed. In fact, it should be noted that in all cases residual benzamide and unreacted aniline was obtained, even with the higher yielding syntheses. One aliphatic *C*-substituents (adamantyl) was prepared *via* route 1 in this study, which afforded **22** in reasonable yield (46%, $R_1 = R_3$ = diethylphenyl). However, when R_1 and R_3 = diisopropylphenyl product formation was hindered, with **14** isolated in just 6% yield, prohibiting further use.

A further limitation of this route is the commercial availability of the carboxylic acid, which whilst varied, in some instances forces a different synthetic approach *e.g.* R_2 = diisopropylphenyl. Conversely, we have been unable to access pro-ligands with mesityl *N*-substituents ($R_1 = R_3$ = mes) *via* route 3 (*vide infra*), however Kays and co-workers have previously reported a series of these compounds *via* route 1.[31] As the *N*-mesityl substituents do not meet the steric tolerance of our system, they will not be discussed further herein. Finally, it is notable that the scale of route 1 is limited, at least in standard chemistry laboratories, due to the considerable excess of PPSE required (for approximately 9 mmol ligand, 5 g P_4O_{10} and 25 mL HMDSO are required), and the associated quenching thereof.§ Route 1 is, however, excellent for the exploratory synthesis of a range of ligands.

For more challenging *C*-substituents, a second synthetic approach was used: route 2 (Scheme 1). Here, the aryl lithium reagent can be prepared, if not commercially available, offering reasonable scope in R_2 substitution. Two drawbacks of this route are the requirement for rigorous air and moisture free conditions due to the reactive nature of the lithium precursor and the limited number of commercially available carbodiimides, restricting *N*-substitution ($R_1 = R_3$ = cyclohexyl, *tert*-butyl, diisopropylphenyl).¶ Route 2 provided pro-ligands **10**, **11** and **12** in good yield. For **10** and **11**, R_2 = *ortho*-xylyl or mesityl, this yield is greatly improved *versus* route 1 (~70% *versus* ~25%), whilst **12** was only prepared *via* route 2 as the carboxylic acid required for route 1 was not readily available (and sterics would likely limit product formation). Whilst **20** could be prepared *via* both routes 1 and 2 (yields: 36% and 17%, respectively), the yield for route 2 was unexpectedly low, potentially due to residual iodine from the synthesis of the carbodiimide.[33] It is also notable that isolation of the lithium aryl is essential for good yields, with any residual *n*-butyllithium (used to form LiAr) competes in the reaction, leading to the undesired formation of the *n*-butyl analogue (R_2 = *n*Bu)[34] and suppression of the overall yield, as observed with the synthesis of **1** *via* route 2 (yield: 38% *vs.* 72% for route 1 and 68% for route 3).

Both route 1 and route 2 offer a relatively simple, one-step synthesis to a wide range of symmetrical pro-ligands. However, asymmetric pro-ligands, where $R_1 \neq R_3$, require a different synthetic approach. Route 3 introduces the *N*-substituents (R_1 and R_3) in separate synthetic steps, as such symmetric and asymmetric pro-ligands can be accessed *via* this route (Scheme 1). The asymmetric pro-ligands **15–18** were formed *via* route 3, and isolated in moderate-very good yields (38–81%). Despite the multistep synthesis, which requires the use of dry solvents, route 3 is highly scalable, with >10 g scale syntheses possible. For pro-ligand **1**, for example, the yield is only slightly reduced using route 3 compared to route 1 (68% *versus* 72%), but it can be prepared on a multigram scale. Route 3 does however have limitations. For example, in our hands, is has not been possible to successfully convert the amide intermediate to pro-ligands, when R_1 = mesityl. However, introducing a mesityl group at R_3 is possible (*e.g.* **18**); note $R_1 = R_3$ = mesityl can be accessed *via* route 1.

Ligand characterisation

Unlike the closely related β-diketimines ("BDI" ligands) or the even closer related guanidines, amidine pro-ligands do not to afford sharp, well resolved ^{1}H NMR spectra in standard laboratory solvents (*e.g.* $CDCl_3$ and benzene-d_6) and to an unfamiliar eye, these compounds might look impure.

The most pronounced example of this is for pro-ligands where R_2 has 2,6-subsitution of an aryl group. For example, significant broadening is observed in the ^{1}H NMR spectrum of pro-ligand **11** (benzene-d_6), which is most pronounced for the *N*-substituents and the amidine proton. Broad multiplets are observed at 1.50–0.68 and 3.92–2.91 ppm in place of the sharp doublet and heptet which are characteristic of diisopropyl groups and two N*H* resonances are observed, at 6.54 and 5.58 ppm, with integrals of approximately 0.66 : 0.33, respectively (Fig. S96). Substituents at the *C*-bridgehead position are relatively less affected by the broadening, and for interpret-

‡ Some of these ligands have been previously reported, see ref. 18, 31 and 49–52.
§ Flask size is also a limiting factor. In our hands, under the reaction conditions, the minimum volume flask required for this synthesis is a 500 mL round-bottom Schlenk, as with smaller volumes after refluxing overnight degradation of the grease was observed and the PPSE leaked from the flask.

¶ Carbodiimides can also be prepared by literature procedures (see SI for further details).[33,53]

ation of the ^{1}H NMR spectra the relative ^{1}H integral ratios may be referenced to these resonances. This effect is replicated in the $^{13}C\{^{1}H\}$ NMR spectra.

Broadening is significantly diminished in the case of ligands without 2,6-aryl substitution of the *C*-bridgehead. For example, **7** has some well-resolved heptets and doublets of doublets, corresponding to the isopropyl groups (Fig. S77). Nevertheless, there are two observed N*H* resonances and broad, minor peaks for most resonances (but not the protons on the *meta*-xylyl substituent).

Further differences are observed between the ^{1}H NMR spectra of these ligands in different solvents, with sharper resonances observed in chloroform-*d* compared to benzene-d_6. The origin of this broadening is likely to be a combination of steric hindrance of the substituents and the tautomerisation between the *E*-, *Z*-, *syn*- and *anti*-tautomers.

The pro-ligands **1–23** are also highly crystalline, and single crystal X-ray diffraction (SCXRD) can be used to confirm absolute structure and conformation. This is especially pertinent for asymmetric ligands where complex NMR spectra can complicate assignment. For example, pro-ligand **12** crystallised from hexane in the *C*2/*c* space group (Fig. 3). In the solid state **12** was found to crystallise in the *anti*-conformation. The *N*-aryl groups are approximately orthogonal to the N–C–N ligand plane and the N*H* proton is observed in a 58 : 42% occupancy on both nitrogen atoms. See SI section 4 for the details of the crystal structures of **5**, **14**, **19** and **20**.

Although the *E*/*Z* *syn*/*anti* isomerism has been well documented,[1,2,23,32,35,36] the notably different NMR spectra observed across our portfolio of pro-ligands prompted us to investigate further. Pro-ligands **7**, **10**, **12** and **22**, chosen to represent a range of substitutions at R_2, were optimised in each possible conformation (E_{syn}, E_{anti}, Z_{syn} and Z_{anti}) in the gas phase (M062x, 6-31G**), benzene and chloroform (PCM), with their relative energies presented in Table S4. The lowest energy conformation varies for each ligand, with the two with 2,6-substituted R_2 groups (**10** and **12**) being most stable in the Z_{anti} conformation, whereas **22** is most stable in the Z_{syn} conformation. **7** is most stable in the E_{syn} conformation (although the Z_{anti} conformation is virtually degenerate). Overall, it is evident that each ligand has several conformations of very similar energy, with no global lowest energy conformation. The several low energy conformations are consistent with the multiple conformations observed *via* ^{1}H NMR spectroscopy.

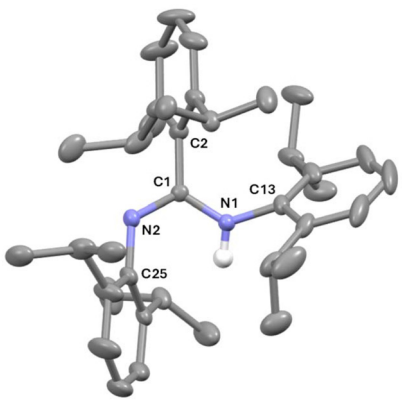

Fig. 3 The solid-state structure of **12** (disorder, hydrogen atoms except N*H* atoms omitted for clarity, ellipsoids 50% probability). For key bond lengths and angles see Table S1. *Note*: route 3 overall yield reported over 2-synthetic steps.

Coordination chemistry

In recent years, our research exploits have led us to utilise amidinate complexes of main group metals in a variety of applications, with aluminium hydrides being a common thread in our synthetic endeavours. We have used amidinate aluminium(III) hydrides as catalysts in hydroboration reactions, reduced them using soluble stoichiometric reducing agents and we also use hydrides as precursors to access other useful Al reagents *e.g.* aluminium(III) iodides.[19] We have found aluminium(III) hydrides, which in most cases can be easily synthesised by reaction of a pro-ligand with the precursor trimethyl amine alane ($AlH_3{\cdot}NMe_3$), to be an excellent gauge for the steric effects ligand variation. Using $AlH_3{\cdot}NMe_3$ it can be challenging to control the stoichiometry (compared to metal halide/ligand salt exchange), with mixtures of mono- and bis-ligated products often observed. Despite the synthetic challenge, this has proved a useful diagnostic tool. Furthermore, the resultant products provide discrete structures that can be used to compare structural features.

We have previously detailed the synthesis and characterisation of the aluminium hydride complexes of ligands **1** and **17**, **18** and **23** (which bear the 'super bulky' aryl group 2,6-bis(diphenylmethyl)-4-methylphenyl).[11,18] Furthermore, syntheses of amidines bearing significantly smaller *C*- and *N*-substituents and complexes of **13** have been reported several times, as such, we will not be discussing them further herein.[37–41] Instead, we will focus on the reaction of pro-ligands where R_1 and R_3 groups = 2,6-diethylphenyl or 2,6-diisopropylphenyl.

Complex synthesis

The mono-ligated aluminium(III) dihydrides, where $R_1 = R_3$ = dipp (Scheme 2, RHS), were synthesised in reasonable to good yields *via* the slow addition of the pro-ligand to a slight excess (1.2 equivalents) of $AlH_3{\cdot}NMe_3$ at −10 °C in toluene. Pro-ligand addition must be slow to inhibit the formation of the bis-ligated species, which is competitive for all but the bulkiest ligands (**10**, **11** and **12**). The pro-ligand with the most sterically bulky R_2 group (**12**) required more forcing conditions, as no ligation was observed at room temperature. Compound **12-Al** was successfully synthesised by reaction of **12** with 2 equivalents of $AlH_3{\cdot}NMe_3$ in toluene at 100 °C overnight. The excess $AlH_3{\cdot}NMe_3$ is required to mitigate competing decomposition at high temperature and despite the high temperature no bis-ligated product was observed.

Heteroatoms also posed issues. The attempted formation of a mono-ligated product though the complexation of **5** with $AlH_3{\cdot}NMe_3$, under the standard reaction conditions (−10 °C,

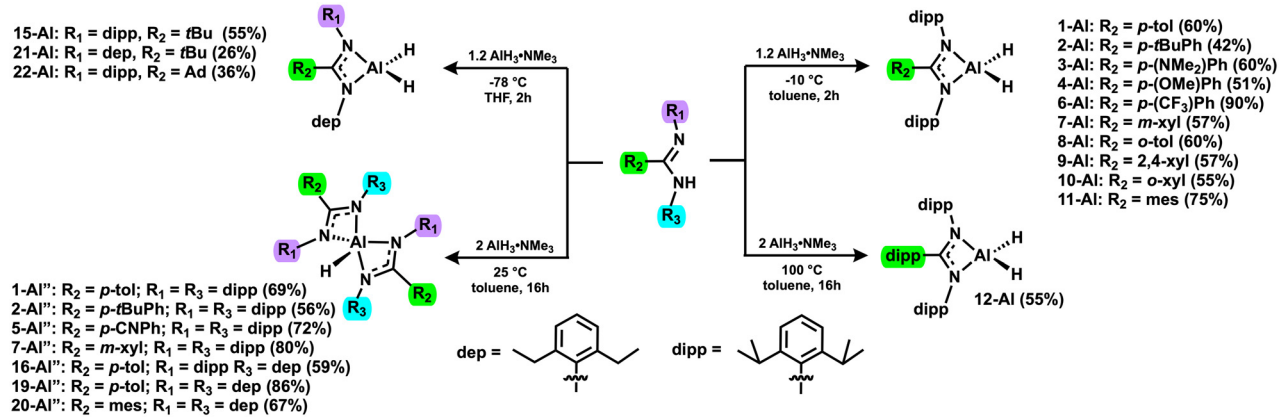

Scheme 2 The reaction of amidine pro-ligands with $AlH_3{\cdot}NMe_3$.

toluene), led to an insoluble brown powder.‖ Conversely, performing the addition at room temperature afforded the bis-ligated **5-Al″** in a yield of 72%.** Meanwhile, although the treatment of **6** afforded predominantly **6-Al** (and small amounts of **6-Al″**), traces of an additional species were observed *via* ^{1}H and $^{19}F\{^{1}H\}$ NMR spectroscopy, indicating some C–F bond activation may have occurred (Fig. S74 and S76).

With the slightly smaller *N*-substituents, R_1 and/or R_3 = diethylphenyl (dep), addition of the pro-ligands to $AlH_3{\cdot}NMe_3$ in toluene at −10 °C or −78 °C afforded the bis-ligated Al exclusively (**16-Al″**, **19-Al″**) or contained substantial (>33%) bis-ligated impurity (pro-ligands **20**, **21** and **22**). An exception here is **15-Al**, which could be isolated cleanly with careful addition of the ligand at −78 °C (55%). The bis-ligated compounds can be directly targeted by reaction of 2 equivalents of **16**, **19** or **20** or with $AlH_3{\cdot}NMe_3$ in toluene at room temperature for 16 hours, affording the bis-ligated species in yields of approximately 80%.

For pro-ligands **20**, **21** and **22**, changing to the coordinating solvent to THF significantly suppressed the formation of the bis-ligated species. As such, compounds **20-Al**, **21-Al** and **22-Al** could be cleanly isolated by reaction of 1 equivalent of pro-ligand with a slight excess of $AlH_3{\cdot}NMe_3$ in THF at −78 °C (90%, 26% and 36%, respectively). However, under the same conditions pro-ligand **19** led only to an intractable mix of the mono- and bis-ligated products.

Whilst their formation is not as competitive, bis-ligated products can also be selectively prepared when R_1 = R_3 = dipp, with the exception of pro-ligands **10**, **11** and **12**. Compounds **1-Al″**, **2-Al″** and **7-Al″**, were all formed through reaction of their respective pro-ligand with 0.5 equivalents of $AlH_3{\cdot}NMe_3$ in toluene at room temperature. Trace amounts of these species were sometimes observed when targeting the mono-ligated species; how problematic this competing product formation is directly correlates with solubility. For example, **1-Al″** is relatively insoluble in toluene (fine white precipitate observed in the reaction) and when preparing **1-Al** it is easily removed by filtration during work-up. Thus, for **1-Al** temperature control during reaction needs not be stringent. However, when attempting to form **2-Al**, the formation of **2-Al″** must be suppressed using cooling and slow addition of ligand to enable clean product formation.

Coordination complexes: NMR characterisation

Unlike the NMR spectra of the pro-ligands, the ^{1}H and $^{13}C\{^{1}H\}$ NMR spectra of the aluminium(III) dihydride species are generally sharp, with high levels of symmetry (all data discussed in benzene-d_6; see SI section 6). Along with more resolved spectra, a further notable difference between the NMR spectra of the pro-ligands and the complexes is the ^{13}C resonance corresponding to the backbone or bridgehead carbon (the N*C*N resonance). In the pro-ligands, this resonance appears between 155–152 ppm, whereas in the complexes a substantial shift is observed upon deprotonation (177–173 ppm). Largely, the NMR spectra are consistent with previously described aluminium hydride complexes, with a single set of resonances corresponding to the amidinate ligands and a broad singlet corresponding to the Al*H*$_2$ moiety. The hydride resonances are generally broad, approximately 0.2 ppm wide, although it is notable that the resonance for **12-Al** is extremely broad (approximately 0.8 ppm wide). The Al–*H* resonance appears between 5.00–5.12 ppm for dipp-*N*-substituted hydrides, whereas for the dep-*N*-substituted and asymmetric hydrides the resonance appears between 4.61–4.69 ppm.

There are notable features to the ^{1}H NMR spectra of some of the aluminium dihydride species. Compounds **10-Al** and **11-Al**, which both have double *ortho* substitution of the R_2 phenyl group, have extremely similar ^{1}H NMR spectra (Fig. S94 and S98). In both cases there is notable broadening of the isopropyl methine and methyl resonances, likely indicating a sterically congested environment restricting free rotation of these groups. In contrast, substantial broadening of the resonances corresponding to the isopropyl groups is not observed

‖Addition of Lewis basic donors such as THF, acetonitrile and dimethylaminopyridine (DMAP) did not render this complex soluble.
**Yield based on the pro-ligand added, 1.2 equivalents of alane added.

for **12-Al** (where R_2 = dipp); instead, each isopropyl group is rendered inequivalent (Fig. S102). The asymmetry imparted when R_2 = *o*-tolyl or 2,4-xylyl manifests with a decrease in symmetry in the ^{1}H NMR spectrum. For compounds **8-Al** and **9-Al** this results in four sets of isopropyl doublets, each integrating to 6H, rather than the two doublets (12H); this is due to the loss of the symmetry about the NCNAl plane (Fig. S86 and S90).

Where $R_1 \neq R_3$ (*e.g.* **15-Al**), as expected two sets of *N*-aryl resonances are observed, and the Al*H* resonance is observed at 4.69 ppm (Fig. S108), closer to that of **21-Al** (4.57 ppm, Fig. S127) than that of **13-Al** (4.87 ppm) but otherwise the ^{1}H NMR spectra are unremarkable.

The NMR spectra of the bis-ligated monohydrides differ substantially from the dihydrides. The most notable difference is the much broader Al*H* resonance, up to 2 ppm wide (rendering them almost imperceptible) and significant inequivalence of the isopropyl- or diethyl-phenyl R_1 and R_3 groups. The latter is likely a result of the greater steric congestion about the metal centre. Comparison of the diagnostic isopropyl resonances of **7-Al** and its bis-ligated congener, **7-Al″**, shows two doublets (12H) and a heptet (2H) for the mono-ligated species (Fig. S79 and S81). Whereas the bis-ligated species has eight doublets and four heptets, with each of the isopropyl groups inequivalent to one another. The effects of this steric congestion are not, however, extended to the *C*-bridgehead, where a singlet (12H) corresponding to the *m*-CH_3 groups is observed.

Crystallographic characterisation

Aluminium(III) dihydrides can all be readily crystallised from the concentrated hydrocarbon solvent solutions at −40 °C for 1–3 days. In general, these hydride species crystallise as either centrosymmetric dimers, with two bridging hydrides and two "terminal" hydrides or, where bulkier aryl groups are used, they may crystallise as monomers (Fig. 4).[18] Crystals of **10-Al**, **11-Al** and **15-Al** suitable for single-crystal X-ray diffraction (SCXRD) were afforded from concentrated hexane solutions at −40 °C, crystals of **20-Al** were grown from the slow evaporation of a saturated hexane solution, and crystals of **4-Al**, **6-Al**, **7-Al**, **9-Al** and **20-Al** were obtained from concentrated toluene solutions at −40 °C. **10-Al** (Fig. 4d) crystallised as a monomer, in the $P\bar{1}$ space group, whereas **11-Al** (Fig. 4e) crystallised in the $I2/a$ space group, with both the monomer and the hydride bridged dimer present in the asymmetric unit, an unpre-

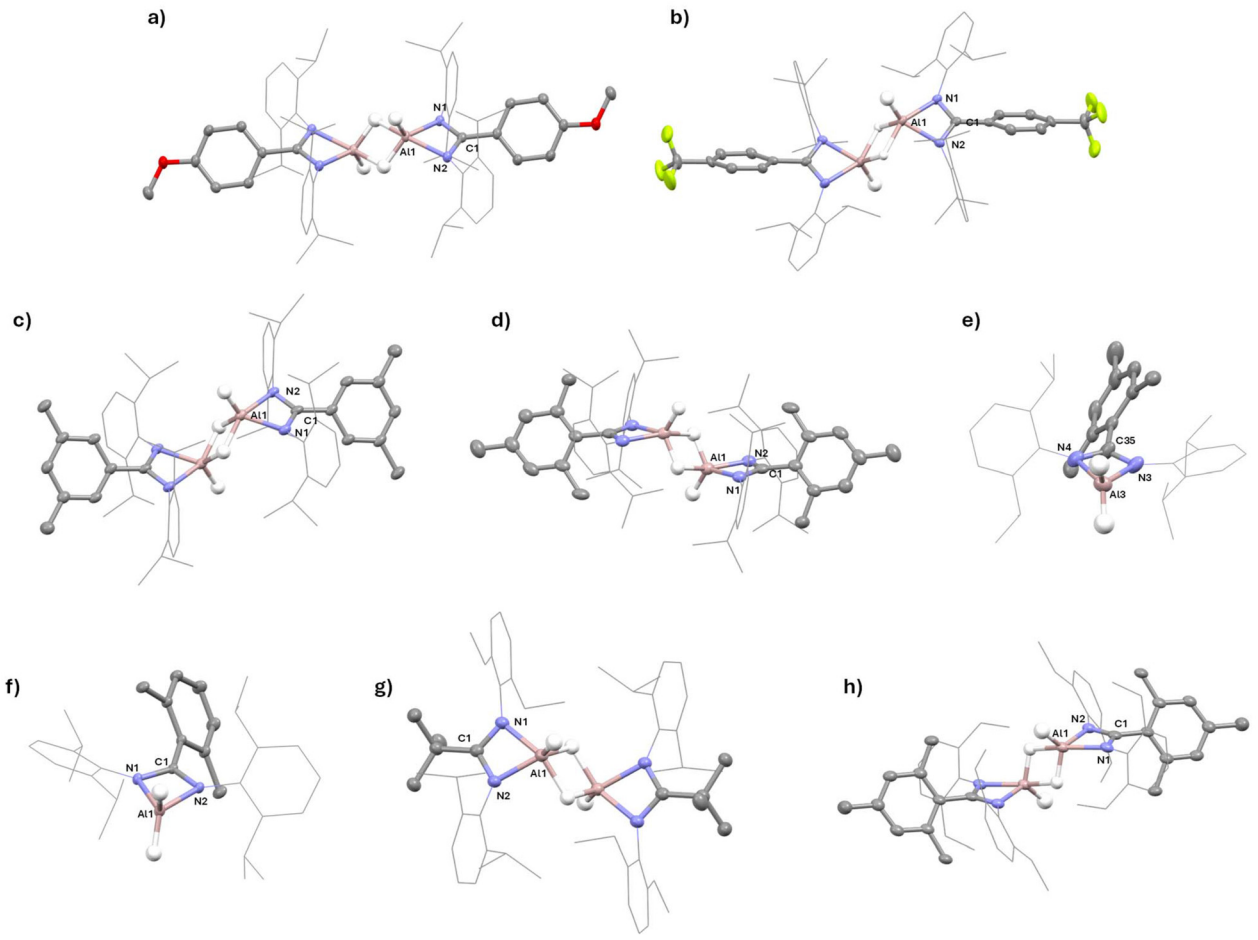

Fig. 4 The solid-state structure of (a) **4-Al-1**, (b) **6-Al**, (c) **7-Al**, (d) **10-Al**, (e) **11-Al-1**, (f) **11-Al-2**, (g) **15-Al** and (h) **20-Al** (*N*-aryl groups wireframe; disorder and hydrogen atoms except Al*H* atoms omitted for clarity, ellipsoids 50% probability). For key bond lengths and angles see Table S2.

cedented phenomenon for these species (see Fig. S17). These two compounds are only the second and third examples of amidinate-stabilised aluminium hydrides crystallising as monomers, the previously reported **23-Al** being the only other example.[18] **4-Al**, **5-Al**, **6-Al** (Fig. 4a–c) and **9-Al** (see SI, Fig. S12–15) all crystallised as dimers, but in the case of **4-Al** and **9-Al** two half dimers are present in the asymmetric unit. **9-Al** co-crystallised with a minor component of the mixed hydride-hydroxide species **9-Al-OH**, with a OH composition of 13% and whilst no significant deviation in bond lengths and angles is observed (see SI Table S2) detailed discussion of the bond lengths and angles has not been carried out for **9-Al**. Species of this type are not unprecedented in aluminium chemistry.[42]

Regardless of crystallisation solvent or aggregation, the aluminium hydride species are effectively isostructural, with the Al centres coordinated it a distorted tetrahedral fashion. For the dimeric species, the Al–N bond distances are marginally longer (mean Al–N bond distance: 1.952 Å) than in the monomers (mean Al–N bond distance: 1.926 Å), but all are consistent with previously observed aluminium hydride species. The asymmetrically substituted **15-Al** (Fig. 4g) exhibits no significant structural differences despite its different *N*-aryl groups. Conversely, **20-Al** (Fig. 4h) exhibits substantial asymmetry in the Al–N bond distances (2.006(3) and 1.912(2) Å for Al–N(1) and Al–N(2), respectively). The twist of the backbone aryl group from the NCN ligand plane varies slightly with aryl substitution. Those without 2,6-substitution exhibit twists of 38–48°, whereas the 2,6-substituted **10-Al** and **20-Al** are twisted approximately 56–60° away from the NCN ligand plane.

Structures of the bis-ligated complexes were also obtained (Fig. 5). **2-Al″** crystallised from the cooling of a concentrated hexane solution in the *P*2/*n* space group (Fig. 5a). **16-Al″** crystallised from a concentrated toluene solution in the *C*2/*c* space group (Fig. 5b), with half a molecule in the asymmetric unit. In both cases, the aluminium hydride moieties were found to be disordered over two positions, with approximately 50 : 50 occupancy for **2-Al″** and 75 : 25 for **16-Al″**. The Al centres adopt a distorted square pyramidal geometry (mean τ_5 values: 0.16 and 0.15 for **2-Al″** and **16-Al″**, respectively), consistent with other reported examples.[18,39,41,43–45] The Al–N bonds are notably lengthened compared to the mono-ligated species (mean Al–N = 2.00 Å *vs.* 1.95 Å), and the bite angle is also somewhat tighter than the other examples.

Structural analysis

It is clear from the SCXRD data that different solid-state structures and crystal packing effects preclude direct comparison of structural features across substituents. As such we opted to use density functional theory (DFT) as a more uniform method of comparing a wide range of subtle structural modifications. The geometries of the aluminium(III) dihydride compounds (**1-Al** to **23-Al**) were optimised in the gas phase (M062X, Al SDDAll, C, H, N 6-31g**); the structures were then used to quantify differences in the steric environment at Al with differing ligand substitution. This was carried out by two methods; firstly by calculation of the buried volume[46,47] and secondly through the use of AtomAccess[48] (Table 1).

Both buried volume and AtomAccess were applied to account for the slightly lower cutoff (3.5 Å from the metal centre) for steric bulk with buried volume. There are some minor discrepancies in trends from buried volume values, compared to AtomAccess, however, overall, these two techniques complement one another nicely. It is worth noting that both buried volume and AtomAccess values varied significantly between data generated from DFT optimised structures *versus* structural parameters derived from SCXRD data, due to dimerisation and packing effects. However, these numbers were much closer for the three complexes that crystalised as monomers (**10-Al**, **11-Al**, **23-Al**).

Upon assessing buried volume and AtomAccess data across the **1-Al** to **23-Al** series (Table 1), it was possible to identify several informative trends.

Firstly, we will look at changes to the R_2 substituent (where R_1 = R_3; dep or dipp). When R_2 is a substituted phenyl ring, the position of substitution is important. Varying the *para* or *meta* substituents has virtually no effect on access to the Al centre, even when significant steric bulk is introduced *e.g.* *p*-*t*Bu (**1-Al** to **7-Al** buried volume 48.9–48.6%). This is a valuable observation as it indicates effects resulting from *para*-substitution are likely to be purely electronic in nature.

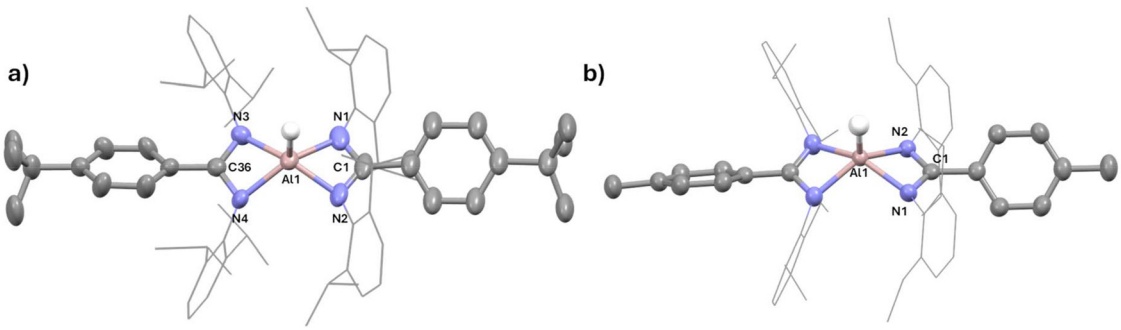

Fig. 5 The solid-state structure of (a) **2-Al″** and (b) **16-Al″** (*N*-aryl groups wireframe; disorder and hydrogen atoms except Al*H* atoms omitted for clarity, ellipsoids 50% probability). For key bond lengths and angles see Table S3.

Table 1 Buried volume and AtomAccess data for complexes **1-Al** to **23-Al** calculated from DFT optimised structures of Al complexes in their monomeric form

Compound	Buried vol. (%)	AtomAccess (%)
1-Al	48.8	48.5
2-Al	48.9	48.3
3-Al	48.8	48.3
4-Al	48.6	48.5
5-Al	48.9	48.5
6-Al	48.8	48.7
7-Al	48.6	48.7
8-Al	49.7	48.0
9-Al	49.7	47.7
10-Al	51.9 [49.9]	45.9 [47.4]
11-Al	51.8 [51.6]	46.1 [48.4[a], 44.5]
12-Al	52.7	44.6
13-Al	50.7	48.2
14-Al	51.7	47.8
15-Al	48.1	51.3
16-Al	46.9	51.5
17-Al	52.8	40.3
18-Al	50.3	44.5
19-Al	48.1	51.8
20-Al	48.6	50.8
21-Al	50.1	49.9
22-Al	50.4	49.7
23-Al	64.9 [66.7]	28.9 [27.4]

Values derived from SCXRD data. [a] Value for dimer.

Substitution at the *ortho* position starts to significantly reduce access to Al, as evidenced in both buried volume and AtomAccess calculations. When R_1 = R_3 = dipp, single *ortho* substitution sees a reduction in access to the Al centre; this is further reduced by double *ortho* substitution *e.g.* mesityl (**1-Al** > **8-Al** > **11-Al**). As may be anticipated, in this series the *ortho* effect peaks when R_2 = 2,6-diisopropylphenyl, which has significantly increased buried volume (52.7%) and reduced atom access (44.6%). This effect is more pronounced when R_1 = R_3 = dipp *versus* dep, indicating that R_2 substitution becomes more important as steric crowding is increased. For example, comparison of **19-Al** (*p*-tol) *versus* **20-Al** (mes) sees a negligible difference in both buried volume and AtomAccess.

Other R_2 substituents in the series can also be compared. When R_1 = R_3 = dipp, an adamantyl *C*-substituent leads to a significantly more hindered Al centre than *tert*-butyl, which is in turn more hindered than phenyl: Ad (**14-Al**) > *t*Bu (**13-Al**) > *p*-tol (**1-Al**). When R_1 = R_3 = dep this trend is slightly less pronounced: Ad (**22-Al**) ≈ *t*Bu (**21-Al**) > *p*-tol (**19-Al**). This further supports R_2 substitution being more influential when R_1 and R_3 are larger. To further highlight this point, *ortho* phenyl *C*-substitution has a similar steric effect to adamantyl when R_1 = R_3 = dipp (**11-Al** *versus* **14-Al**), but when R_1 = R_3 = dep, it is more comparable to the *para*-tolyl substituent (**19-Al** *versus* **20-Al**).

As anticipated, in all cases access to the Al centre is more restricted when R_1 = R_3 = dipp *versus* R_1 = R_3 = dep. However, the magnitude of the steric influence strongly depends on R_2, as detailed above. And thus, it follows that when the size of both the R_1 and R_3 groups is significantly increased, a marked reduction in access to the Al centre is observed (**23-Al**, R_1 = R_3 = 2,6-bis(diphenylmethyl)-4-methylphenyl).

Finally, the introduction of asymmetry into the ligand framework ($R_1 \neq R_3$) increases access to the Al centre. This is observed when R_2 = *tert*-butyl and *para*-tolyl, where in both cases the % buried volume is significantly smaller when R_1 = dep and R_3 = dipp, *versus* the symmetric equivalents (*t*Bu: **15-Al** < **21-Al** ≈ **13-Al**; *p*-tol: **16-Al** < **19-Al** ≈ **1-Al**).

In addition to using the DFT data to assess structural parameters, the HOMO–LUMO gaps were also analysed for all the species at the same level of theory to quantify the electronic effects (if any) of the ligand modification. Despite its profound effect on the sterics and subsequently the coordination chemistry, variation of the *N*-aryl group appears to have no significant effect. Comparing **1-Al** (R_1 = R_3 = dipp, HOMO–LUMO gap: 6.55 eV) to **19-Al** (R_1 = R_3 = dep, HOMO–LUMO gap: 6.56 eV), a difference of less than 0.01 eV in the HOMO–LUMO gap was observed (although, a slight increase in the HOMO–LUMO gap is observed for the "superbulky" **23-Al**, with a HOMO–LUMO gap of 6.99 eV). Conversely, variation in the *C*-substituent (R_2) leads to more significant effects. The mean HOMO–LUMO gap for aryl substitution is 6.66 eV, whereas for alkyl substitution it is 7.78 eV, a difference of almost 1.2 eV. Between the substituted aryl examples, little variation in the HOMO–LUMO gaps is observed across the electron donating substituents, however the two examples with electron withdrawing substituents (**5-Al** and **6-Al**) present slightly contracted HOMO–LUMO gaps (5.97 and 6.26 eV, respectively) compared to the mean value. For full results see SI.

Conclusions

In summary, the synthesis of a range of symmetric and asymmetric amidine ligands, with a variety of steric constraints at the R_1, R_2 and R_3 positions, have been presented. Three different routes have been used in the preparation of this series, with the benefits and drawbacks to each route discussed. This is the first time such synthetic details have been collated in one place for a wide range of compounds.

The steric properties of these ligands have been probed *via* their use as supporting ligands for the synthesis of a range of amidinate aluminium hydride species. Less bulky amidinate ligands readily afforded bis-ligated species (***n*-Al″**), but the bulkier ligands afforded mono-ligated aluminium dihydrides (***n*-Al**), though in most cases product formation could be controlled though judicious choice of solvent and temperature. The aluminium hydride complexes have been characterised using multinuclear NMR techniques and, in several cases, SCXRD.

To facilitate structural comparison of the compound series, we optimised geometries using DFT, and through a combination of these results, and SCXRD data where appropriate, calculated % buried volume and AtomAccess calculations. From this data we were able to assess the effects of varying ligand substitution on the steric environment around Al.

It is our hope that the results presented herein provide a valuable resource for those wishing to employ amidine ligands in their research, allowing selection of synthetically accessible compounds with prior knowledge of their relative steric properties.

Author contributions

M. d. V. T.: investigation, formal analysis, crystallography, validation, data curation, computational analysis, writing – original draft. I. S.: investigation, crystallography, validation, data curation. M. T.: investigation, formal analysis, computational analysis. R. A.: investigation, formal analysis. T. S.: investigation. D. U.: investigation. G. A.: computational analysis. L. S. M.: crystallographic validation. C. B.: writing, visualisation, supervision, funding acquisition, conceptualisation.

Conflicts of interest

There are no conflicts to declare.

Data availability

All data to support the study are included in the supplementary information (SI), or uploaded to the relevant data repositories.

Supplementary information: data for single crystal X-ray diffraction experiments; DFT coordinates for the calculations in the form of a XYZ text file; NMR spectra of all compounds isolated. See DOI: https://doi.org/10.1039/d6dt00276e.

Raw NMR data files are available upon request.

CCDC 2527288–2527303 contain the supplementary crystallographic data for this paper.[54a–p]

Acknowledgements

C. B. thanks the Engineering and Physical Sciences Research Council (grant number EP/Y000129/1) for funding. King's College London NetZero centre is thanked for studentship funding (M. T.). Jeremy Cockcroft (UCL) and Jens Najorka (NHM, grant number NE/X005992/1) are thanked for helping us access SCXRD. Thomas Hicks and the CBS NMR Facility are thanked for support running NMR spectroscopy experiments.

References

1 J. Barker and M. Kilner, *Coord. Chem. Rev.*, 1994, **133**, 219–300.
2 M. P. Coles, *Dalton Trans.*, 2006, 985.
3 D. Sengupta, A. Gómez-Torres and S. Fortier, in *Comprehensive Coordination Chemistry III*, Elsevier, 2021, vol. 1–9, pp. 366–405.
4 F. T. Edelmann, in *Advances in Organometallic Chemistry*, 2008, pp. 183–352.
5 M. Cortijo, R. González-Prieto, S. Herrero, J. L. Priego and R. Jiménez-Aparicio, *Coord. Chem. Rev.*, 2019, **400**, 213040.
6 S. Nagendran and H. W. Roesky, *Organometallics*, 2008, **27**, 457–492.
7 Y. Zhang, L. Wu and H. Wang, *J. Am. Chem. Soc.*, 2022, **144**, 22446–22450.
8 M. Y.-S. Wee, S. Quek, C.-S. Wu, M.-D. Su and C.-W. So, *J. Am. Chem. Soc.*, 2024, **146**, 14410–14415.
9 A. Kostenko and M. Driess, *J. Am. Chem. Soc.*, 2018, **140**, 16962–16966.
10 S. Inoue, J. D. Epping, E. Irran and M. Driess, *J. Am. Chem. Soc.*, 2011, **133**, 8514–8517.
11 S. J. Bonyhady, D. Collis, G. Frenking, N. Holzmann, C. Jones and A. Stasch, *Nat. Chem.*, 2010, **2**, 865–869.
12 X. Sun, T. Simler, R. Yadav, R. Köppe and P. W. Roesky, *J. Am. Chem. Soc.*, 2019, **141**, 14987–14990.
13 X. Chen, G.-X. Wang, Z.-J. Lv, J. Wei and Z. Xi, *J. Am. Chem. Soc.*, 2024, **146**, 17624–17628.
14 R. Kretschmer, *Chem. – Eur. J.*, 2020, **26**, 2099–2119.
15 T. Chlupatý and A. Růžička, *Coord. Chem. Rev.*, 2016, **314**, 103–113.
16 S. K. Thakur, J. Langer, N. Roig, A. G. Patro, M. A. Schmidt, M. Alonso and S. Harder, *Angew. Chem., Int. Ed.*, 2026, e25777.
17 C. Bakewell, *Dalton Trans.*, 2020, **49**, 11354–11360.
18 K. Hobson, C. J. Carmalt and C. Bakewell, *Inorg. Chem.*, 2021, **60**, 10958–10969.
19 I. Squire, M. de Vere-Tucker, M. Tritto, L. Silva de Moraes, T. Krämer and C. Bakewell, *Nat. Commun.*, 2026, **17**, 1732.
20 C. Bakewell, K. Hobson and C. J. Carmalt, *Angew. Chem., Int. Ed.*, 2022, **61**, 2–7.
21 I. Squire, M. Tritto, J. Morell and C. Bakewell, *Chem. Commun.*, 2024, **60**, 12908–12911.
22 N. Nimitsiriwat, V. C. Gibson, E. L. Marshall, P. Takolpuckdee, A. K. Tomov, A. J. P. White, D. J. Williams, M. R. J. Elsegood and S. H. Dale, *Inorg. Chem.*, 2007, **46**, 9988–9997.
23 R. T. Boeré, V. Klassen and G. Wolmershäuser, *J. Chem. Soc., Dalton Trans.*, 1998, 4147–4154.
24 F. Qian, K. Liu and H. Ma, *Dalton Trans.*, 2010, **39**, 8071–8083.
25 S. Dagorne, I. A. Guzei, M. P. Coles and R. F. Jordan, *J. Am. Chem. Soc.*, 2000, **122**, 274–289.
26 M. P. Coles, D. C. Swenson, R. F. Jordan and V. G. Young, *Organometallics*, 1997, **16**, 5183–5194.
27 M. Kakimoto, S. Ogata, A. Mochizuki and Y. Imai, *Chem. Lett.*, 1984, **13**, 821–824.
28 S. Ogata, A. Mochizuki, M. Kakimoto and Y. Imai, *Bull. Chem. Soc. Jpn.*, 1986, **59**, 2171–2177.
29 Y. Luo, X. Wang, J. Chen, C. Luo, Y. Zhang and Y. Yao, *J. Organomet. Chem.*, 2009, **694**, 1289–1296.
30 S. Bambirra, D. van Leusen, A. Meetsma, B. Hessen and J. H. Teuben, *Chem. Commun.*, 2003, 522–523.

31 G. J. Moxey, F. Ortu, L. Goldney Sidley, H. N. Strandberg, A. J. Blake, W. Lewis and D. L. Kays, *Dalton Trans.*, 2014, **43**, 4838–4846.
32 J. A. R. Schmidt and J. Arnold, *J. Chem. Soc., Dalton. Trans.*, 2002, 2890–2899.
33 T. Peddarao, A. Baishya, M. K. Barman, A. Kumar and S. Nembenna, *New J. Chem.*, 2016, **40**, 7627–7636.
34 T. Chlupatý, Z. Padělková, A. Lyčka and A. Růžička, *J. Organomet. Chem.*, 2011, **696**, 2346–2354.
35 *Amidines and Imidates*, ed. S. Patai and Z. Rappoport, Wiley, 1991, vol. 2.
36 G. A. Dushenko, I. E. Mikhailov and V. I. Minkin, *Russ. J. Gen. Chem.*, 2020, **90**, 7–12.
37 M. L. Cole, C. Jones, P. C. Junk, M. Kloth and A. Stasch, *Chem. – Eur. J.*, 2005, **11**, 4482–4491.
38 B. Lyhs, D. Bläser, C. Wölper and S. Schulz, *Chem. – Eur. J.*, 2011, **17**, 4914–4920.
39 M. Zhong, Y. Liu, S. Kundu, N. Graw, J. Li, Z. Yang, R. Herbst-Irmer, D. Stalke and H. W. Roesky, *Inorg. Chem.*, 2019, **58**, 10625–10628.
40 A. L. Brazeau, Z. Wang, C. N. Rowley and S. T. Barry, *Inorg. Chem.*, 2006, **45**, 2276–2281.
41 R. Duchateau, A. Meetsma and J. H. Teuben, *Chem. Commun.*, 1996, **86**, 223–224.
42 J. Hicks, A. Heilmann, P. Vasko, J. M. Goicoechea and S. Aldridge, *Angew. Chem., Int. Ed.*, 2019, **58**, 17265–17268.
43 C. Jones, P. C. Junk, M. Kloth, K. M. Proctor and A. Stasch, *Polyhedron*, 2006, **25**, 1592–1600.
44 P. Pallister, J. Pallister, H. Dao, G. Yap and S. Barry, *CSD Commun.*, 2020, DOI: 10.5517/ccdc.csd.cc13fc74.
45 M. L. Cole, A. I. McKay and N. S. Ping, *Polyhedron*, 2019, **170**, 424–430.
46 A. Poater, B. Cosenza, A. Correa, S. Giudice, F. Ragone, V. Scarano and L. Cavallo, *Eur. J. Inorg. Chem.*, 2009, **2009**, 1759–1766.
47 L. Falivene, Z. Cao, A. Petta, L. Serra, A. Poater, R. Oliva, V. Scarano and L. Cavallo, *Nat. Chem.*, 2019, **11**, 872–879.
48 G. K. Gransbury, S. C. Corner, J. G. C. Kragskow, P. Evans, H. M. Yeung, W. J. A. Blackmore, G. F. S. Whitehead, I. J. Vitorica-Yrezabal, M. S. Oakley, N. F. Chilton and D. P. Mills, *J. Am. Chem. Soc.*, 2023, **145**, 22814–22825.
49 C. Jones, S. J. Bonyhady, N. Holzmann, G. Frenking and A. Stasch, *Inorg. Chem.*, 2011, **50**, 12315–12325.
50 M. P. Coles, D. C. Swenson, R. F. Jordan and V. G. Young, *Organometallics*, 1998, **17**, 4042–4048.
51 A. Causero, G. Ballmann, J. Pahl, H. Zijlstra, C. Färber and S. Harder, *Organometallics*, 2016, **35**, 3350–3360.
52 K. B. Aubrecht, K. Chang, M. A. Hillmyer and W. B. Tolman, *J. Polym. Sci., Part A: Polym. Chem.*, 2001, **39**, 284–293.
53 M. Urban, P. H. Marek-Urban, K. Durka, S. Luliński, P. Pander and A. P. Monkman, *Angew. Chem., Int. Ed.*, 2023, **62**, e202217530.
54 (*a*) CCDC 2527288: Experimental Crystal Structure Determination, 2026, DOI: 10.5517/ccdc.csd.cc2qtvfv; (*b*) CCDC 2527289: Experimental Crystal Structure Determination, 2026, DOI: 10.5517/ccdc.csd.cc2qtvgw; (*c*) CCDC 2527290: Experimental Crystal Structure Determination, 2026, DOI: 10.5517/ccdc.csd.cc2qtvhx; (*d*) CCDC 2527291: Experimental Crystal Structure Determination, 2026, DOI: 10.5517/ccdc.csd.cc2qtvjy; (*e*) CCDC 2527292: Experimental Crystal Structure Determination, 2026, DOI: 10.5517/ccdc.csd.cc2qtvkz; (*f*) CCDC 2527293: Experimental Crystal Structure Determination, 2026, DOI: 10.5517/ccdc.csd.cc2qtvl0; (*g*) CCDC 2527294: Experimental Crystal Structure Determination, 2026, DOI: 10.5517/ccdc.csd.cc2qtvm1; (*h*) CCDC 2527295: Experimental Crystal Structure Determination, 2026, DOI: 10.5517/ccdc.csd.cc2qtvn2; (*i*) CCDC 2527296: Experimental Crystal Structure Determination, 2026, DOI: 10.5517/ccdc.csd.cc2qtvp3; (*j*) CCDC 2527297: Experimental Crystal Structure Determination, 2026, DOI: 10.5517/ccdc.csd.cc2qtvq4; (*k*) CCDC 2527298: Experimental Crystal Structure Determination, 2026, DOI: 10.5517/ccdc.csd.cc2qtvr5; (*l*) CCDC 2527299: Experimental Crystal Structure Determination, 2026, DOI: 10.5517/ccdc.csd.cc2qtvs6; (*m*) CCDC 2527300: Experimental Crystal Structure Determination, 2026, DOI: 10.5517/ccdc.csd.cc2qtvt7; (*n*) CCDC 2527301: Experimental Crystal Structure Determination, 2026, DOI: 10.5517/ccdc.csd.cc2qtvv8; (*o*) CCDC 2527302: Experimental Crystal Structure Determination, 2026, DOI: 10.5517/ccdc.csd.cc2qtvw9; (*p*) CCDC 2527303: Experimental Crystal Structure Determination, 2026, DOI: 10.5517/ccdc.csd.cc2qtvxb.